

The Interplay of Vegetation and Land-Atmosphere Feedbacks in Flash Drought Prediction



Mahmoud Osman^{*1,2,3}; Benjamin Zaitchik⁴; Patricia Lawston-Parker^{2,5}; Joseph Santanello⁵; Martha Anderson⁶

¹*Terrestrial Information Systems Laboratory, NASA Goddard Space Flight Center, Greenbelt, MD, USA*

²*Earth System Science Interdisciplinary Center, University of Maryland, College Park, MD, USA*

³*Irrigation and Hydraulics Department, Cairo University, Cairo, Egypt*

⁴*Department of Earth and Planetary Sciences, Johns Hopkins University, Baltimore, MD, USA*

⁵*Hydrological Sciences Laboratory, NASA Goddard Space Flight Center, Greenbelt, MD, USA*

⁶*Hydrology and Remote Sensing Laboratory, Agricultural Research Service, USDA, Beltsville, MD, USA*

**Corresponding author: Mahmoud Osman (Email: mahosman01@gmail.com; mahmoud.a.osman@nasa.gov; mosman1@umd.edu)*

Abstract

Flash droughts, known for their rapid onset and intensification, pose a significant threat to agriculture and water resources. The 2011 Texas flash drought, with its widespread agricultural losses exceeding \$7.6 billion and severe ecological consequences, was a stark demonstration of their devastating impacts. This study investigates the crucial role of vegetation in numerical modeling of flash droughts, focusing on the 2011 Texas event. Utilizing the NASA Unified Weather Research and Forecasting (NU-WRF) and NASA Land Information System (LIS) modeling frameworks and the Noah Multi-Parameterization (Noah-MP) land surface model, we examine the influence of vegetation dynamics on simulating drought characteristics. By integrating satellite-derived vegetation observations and conducting controlled numerical experiments, we evaluate the model's ability to reproduce observed features of the 2011 drought. Our findings underscore the importance of vegetation representation in capturing the complex land-atmosphere feedbacks that drive the evolution of flash droughts. The incorporation of observed vegetation anomalies into the model leads to improved simulations of surface energy fluxes, atmospheric warming, and evapotranspiration patterns, particularly during the crucial onset and intensification phases of the drought. This points to the potential importance of representing vegetation variability in dynamically-based forecasts of flash drought.

Early Online Release: This preliminary version has been accepted for publication in *Journal of Hydrometeorology*, may be fully cited, and has been assigned DOI 10.1175/JHM-D-25-0074.1. The final typeset copyedited article will replace the EOR at the above DOI when it is published.

Introduction

Flash droughts, characterized by their rapid onset and intensification, pose a significant threat to agriculture and water resources (Osman et al. 2021, 2022a; Otkin et al. 2018; Pendergrass et al. 2020; Svoboda et al. 2002). The swiftness of their development, often triggered by a combination of precipitation deficits and anomalous atmospheric conditions such as heat waves and high evaporative demand, makes them particularly difficult to predict and mitigate (Otkin et al. 2013; Yuan et al. 2018; Zhang et al. 2017). The complex interplay between land surface processes and atmospheric conditions during flash droughts underscores the potentially critical role of vegetation in modulating these events (Jiang et al. 2024; Osman et al. 2022a,b). Vegetation, through transpiration and its influence on surface energy fluxes, actively participates in land-atmosphere feedback loops that can either amplify or dampen drought conditions (Arsenault et al. 2018; Osman et al. 2022b; Chiang et al. 2018; Seneviratne et al. 2010; Miralles et al. 2019). However, many operational forecasting systems, particularly subseasonal-to-seasonal (S2S) models, lack a dynamic representation of vegetation, limiting their ability to accurately simulate the intricate feedbacks that govern flash drought intensification (Pendergrass et al. 2020). The accurate representation of vegetation dynamics is crucial across various modeling time scales, from short-term numerical weather prediction (NWP) to longer-term climate models for enhancing flash drought prediction and early warning capabilities.

Recent studies have highlighted the complex impact of vegetation on flash drought development and evolution. For instance, research has shown that the presence of vegetation can influence soil moisture depletion rates, with densely vegetated areas exhibiting higher susceptibility to flash droughts due to increased evapotranspiration under hot and dry conditions, directly driving the surface water balance towards low moisture conditions (Jiang et al. 2024; Zhang et al. 2021). At the same time, it is also possible that dense vegetation can, in some cases, access deeper soil moisture reserves, potentially mitigating the impact of near-surface drying. Additionally, the type and health of vegetation can affect the surface energy balance, altering the partitioning between sensible and latent heat fluxes and potentially amplifying atmospheric warming and drought intensification (Osman et al. 2022b; Miralles et al. 2019). The dynamic nature of vegetation, including changes in leaf area index (LAI) and the complex response of stomatal conductance to water stress, can further modulate land-atmosphere feedbacks during flash droughts (Niu et al.

2011; Parazoo et al. 2024). These vegetation-driven feedbacks can influence atmospheric circulation patterns, cloud formation, and precipitation, potentially leading to self-propagating droughts where initial soil moisture deficits trigger a cascade of atmospheric and land surface drying (Koster et al. 2019; Schumacher et al. 2022; Miralles et al. 2019; Entekhabi 2023).

The critical role of vegetation in flash droughts is further emphasized by studies demonstrating the limitations of models that rely on climatological vegetation inputs. The use of climatological vegetation, instead of dynamic vegetation, is a simplification that can hinder all models and forecast lead times to a struggle to capture the interannual variability of evapotranspiration and land water and energy states. In this study we are concerned with the impact this simplification has for S2S prediction, but it also creates challenges for NWP and climate models attempting to simulate rapidly emerging drought conditions and their feedback on vegetation growth and health (Ukkola et al. 2016a,b; Tallaksen and Stahl 2014). Consequently, the integration of remotely sensed vegetation observations, such as LAI, into land surface models has shown promise in improving drought characterization. Mocko et al. (2021) demonstrated that assimilating LAI data into the Noah-MP land surface model led to substantial improvements in simulating agricultural drought. Similarly, Nie et al. (2022) and Fallah et al. (2024) highlighted the benefits of LAI assimilation in capturing the spatial distribution of vegetation response to drought and improving the simulation of transpiration and associated carbon fluxes and potential transition to longer-term droughts. Furthermore, Ahmad et al. (2022) emphasized the necessity of incorporating multiple observational constraints, including both soil moisture and vegetation properties, to effectively capture the rapid onset and intensification of flash droughts driven by different mechanisms. They also highlighted the importance of capturing the "flashiness" of these droughts, characterized by rapid rates of soil moisture decline and vegetation stress.

The 2011 Texas flash drought, marked by its exceptional intensity and widespread impacts, serves as a compelling case study for investigating the role of vegetation in flash drought modeling (Nielsen-Gammon 2012). While the overall event resulted in the driest 12-month period on record for the state, with an average of slightly more than 11 inches of rainfall compared to the normal 27-inch average (Nielsen-Gammon 2012), it was the rapid onset and intensification within this period that defines the flash drought. This intensification was primarily driven by a persistent lack of precipitation coupled with record-breaking temperatures (Nielsen-Gammon 2012). The severity

of the drought was amplified by antecedent wet conditions in the spring of 2011, which promoted lush vegetation growth that subsequently dried out, providing ample fuel for devastating wildfires and exacerbating soil moisture depletion (Nielsen-Gammon 2012; Schwantes et al. 2016; Yang 2013; Adhikari et al. 2024). The agricultural sector experienced catastrophic losses, exceeding \$7.62 billion, due to widespread crop failures, reduced livestock productivity, and increased supplemental feeding costs (Nielsen-Gammon 2012). The ecological repercussions were also severe, with extensive tree mortality observed across central and eastern Texas, impacting both managed and natural ecosystems (Lawal et al. 2024; Nielsen-Gammon 2012). The drought's intensity was unprecedented, with the Palmer Drought Severity Index (PDSI), a comprehensive measure of drought intensity, reaching record-low values, surpassing even the infamous drought of the 1950s in its severity (Nielsen-Gammon 2012). The extreme heat during the summer months further intensified drought conditions, contributing to the rapid depletion of soil moisture and surface water resources, and highlighting the complex interplay between meteorological, agricultural, and hydrological drought (Nielsen-Gammon 2012; Wilhite et al. 2007).

While the 2011 Texas drought aligns with some characteristics of a 'heat wave flash drought' as defined by Mo and Lettenmaier (2015), our model and satellite derived evapotranspiration observations did not reveal the widespread increase in evapotranspiration (ET) typically associated with the heatwave-driven flash drought events (Osman et al. 2022a). This suggests that other factors, beyond simply high temperatures driving increased ET, played a more dominant role in the rapid soil moisture depletion observed, which emphasizes the different classes and pathways for the onset of flash droughts (Osman et al. 2022a). The Southern Great Plains, characterized by its strong land-surface-atmosphere coupling, is particularly susceptible to such rapid drought intensification, as changes in vegetation and soil moisture can quickly feedback into the atmosphere, influencing temperature, humidity, and ultimately precipitation patterns (Basara and Christian 2018; Koster et al. 2004). This region's location in a transitional zone between humid and arid climates, coupled with its extensive agricultural land cover and reliance on rain-fed agriculture, further amplifies its vulnerability to flash droughts (Koster et al. 2004).

In this study, we delve into the influence of vegetation on the numerical modeling of flash droughts, using the 2011 Texas event as a case study. We leverage the NU-WRF (Peters-Lidard et al. 2007, 2015) and LIS modeling frameworks (Kumar et al. 2006) and the Noah-MP land surface

model (Niu et al. 2011; Yang et al. 2011) to examine the role of vegetation feedbacks on the atmosphere in simulating the onset, severity, and land-atmosphere feedbacks associated with this flash drought. We do this by integrating satellite-derived vegetation observations and conducting controlled numerical experiments with modified vegetation parameters—that is, rather than using a dynamic vegetation model, we prescribe vegetation condition based on satellite-derived observations. This has the advantage of allowing us to look at model sensitivity to observed vegetation stress rather than relying on the model’s own vegetation model to simulate drought impacts on vegetation health. By doing this, we aim to rigorously evaluate the model's ability to reproduce the observed characteristics of the 2011 Texas flash drought. Through a deeper understanding of the role of vegetation as a mediator of flash drought, we can pave the way for the development of more effective strategies to mitigate the impacts of these devastating events on agriculture, water resources, and ecosystems in the Southern Great Plains and beyond.

Methods

The NASA Unified-Weather Research and Forecasting (NU-WRF) model is a fully coupled modeling system designed to simulate the complex, two-way interactions between the atmosphere, land surface, aerosols, clouds, and precipitation at both satellite scales and the process level (Peters-Lidard et al. 2015). It builds upon the widely-used Weather Research and Forecasting (WRF) model (Skamarock et al. 2021), incorporating key NASA capabilities to enhance its representation of Earth system processes.

Crucially for our study on flash droughts, NU-WRF tightly couples the NASA Land Information System (LIS), a high-performance land surface modeling framework, with the WRF atmospheric model. This coupling enables a two-way exchange of information between the land surface model (LSM) and the atmosphere (Peters-Lidard et al. 2015), where the LSM provides best representation of surface fluxes to the atmosphere, and the atmospheric model provides the meteorological forcing for the LSM. This two-way coupling, a central feature of our experimental design, is essential for capturing the dynamic feedbacks that drive the rapid onset and intensification of flash droughts, particularly in regions like the Southern Great Plains where land-atmosphere interactions play a critical role. Furthermore, NU-WRF integrates the Noah-MP land surface model - which is used in both the coupled and offline simulation - allowing for the explicit representation of vegetation dynamics and their influence on soil moisture and surface energy fluxes.

By combining these advanced capabilities, NU-WRF provides a powerful platform for investigating the influence of vegetation on flash drought modeling. The model's ability to integrate satellite-derived vegetation observations and conduct controlled experiments with modified vegetation parameters allows us to rigorously evaluate its performance in simulating the 2011 Texas flash drought and gain deeper insights into the role of vegetation in these extreme events.

The study focuses on the Southern Great Plains (SGP) region, including the state of Texas, USA as shown in Figure 1. This region is characterized by its diverse land cover, ranging from semi-arid grasslands in the west to humid forests in the east. The SGP experiences a continental climate with hot summers and mild winters, making it prone to extreme weather events such as heat waves and

droughts. The 2011 Texas flash drought, which severely impacted the region's agriculture, water resources, and ecosystems, serves as the focal point of this study. The region's strong land-surface-atmosphere coupling, where changes in vegetation and soil moisture can influence the surface fluxes that drive boundary layer evolution and atmospheric conditions (Dirmeyer 2011), makes it a particularly challenging but relevant environment for investigating the role of vegetation in flash drought modeling (Basara and Christian 2018; Koster et al. 2004).

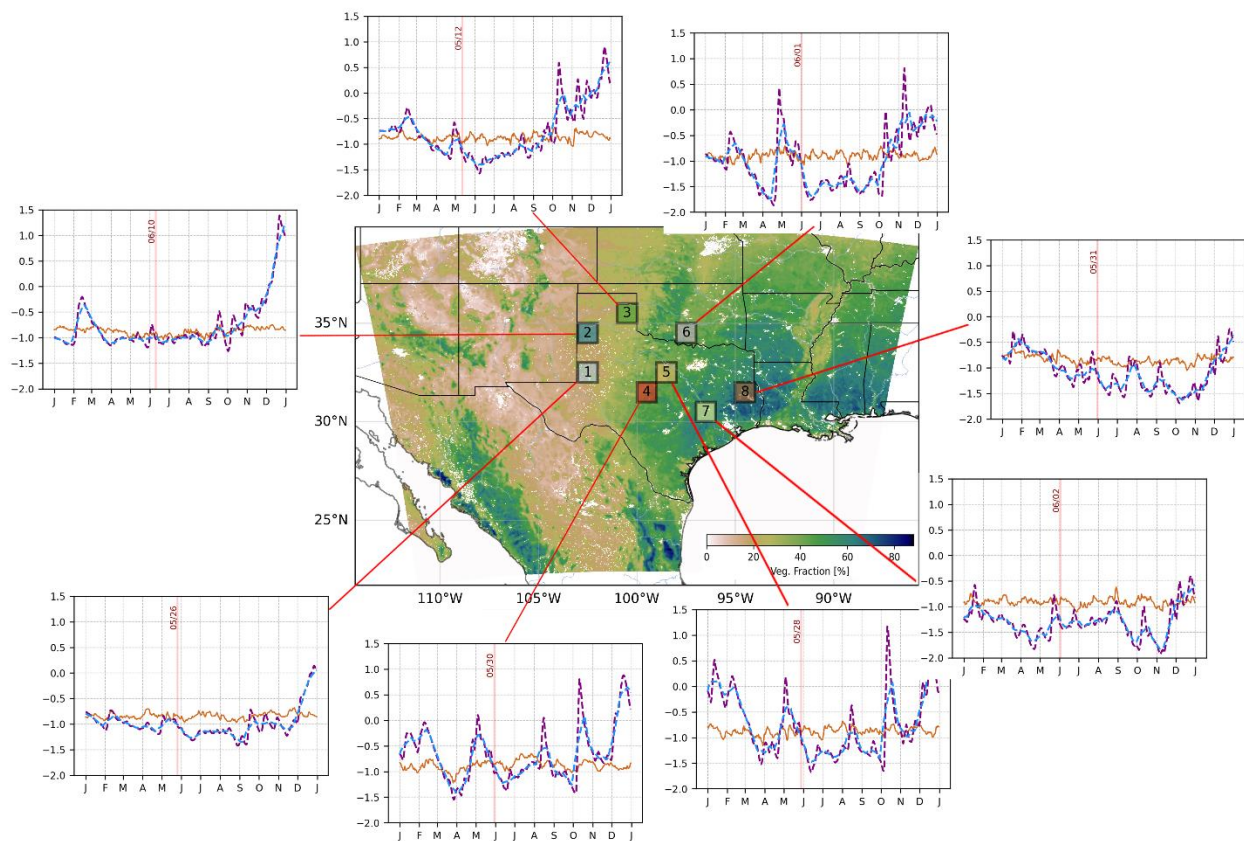


Figure 1: Map of the study domain encompassing the state of Texas, with eight analysis boxes highlighted and numbered. The colors of these boxes correspond to the colors used to represent each box in subsequent figures. The background depicts the climatological annual mean green vegetation fraction (GVF) derived from MODIS observations, illustrating the spatial distribution of vegetation cover across the region. Line-plots next to boxes represent the average flash drought onset date for grid points within each box, as defined using the SMVI flash drought index (Osman et al., 2024). The average flash drought onset dates for grid cells within each box are marked with

the vertical lines. Brown timeseries represent the 20th percentile Root Zone Soil Moisture (RZSM). Purple and blue dashed-lines represent the 5 and 20 days running RZSM averages respectively; Y-axis is the standardized RZSM anomaly.

To capture the spatial heterogeneity of land-atmosphere interactions within this domain, we define eight 1° by 1° analysis boxes (Figure 1), each representing a distinct geographical area with potentially varying vegetation cover, including shrublands, savannas, grasslands, croplands, and sparsely vegetated areas, within the detected flash drought regions during the 2011 event. We excluded other land cover types, such as forests, urban or water, as these selected types are more directly relevant to agricultural drought, the primary focus of this study. These boxes, strategically placed across the state of Texas, allow us to examine regional differences due to the influence of vegetation status on flash drought intensification. The onset date for flash drought in each box is drawn from our previously published inventory of flash droughts (Osman et al., 2024). Briefly, Osman et al. (2024) defined flash drought onset based on a rapid decline in soil moisture, exceeding a specified threshold within a short period. It is important to note that the dates shown in Figure 1 represent the median flash drought onset date for grid points within each box, reflecting the average timing of the event across the region, not a single, synchronous onset.

The model domain was configured with 60 vertical levels, covering a large portion of the Southern Great Plains and surrounding areas at a 4-km horizontal resolution (covering approximately 2500km by 2000km), capturing mesoscale features and regional variations in land surface and atmospheric conditions while allowing for explicit representation of convection. The simulation period extends from March 1, 2011, to August 1, 2011, encompassing the antecedent conditions leading up to and the peak intensification of the 2011 Texas flash drought event. Lateral boundary conditions are drawn from Modern-Era Retrospective analysis for Research and Applications, Version 2 (MERRA-2) reanalysis data, which provides a comprehensive reanalysis of the global atmosphere, land surface, and ocean state, combining satellite observations with a numerical model to generate a consistent and continuous record of meteorological variables (Gelaro et al. 2017).

To ensure an accurate representation of the land surface states at the beginning of the coupled simulation, we conducted an initial 40-year spin-up run using LIS offline, driven by MERRA-2

reanalysis data. This spin-up process allows the land surface model to reach a state of equilibrium, minimizing the influence of initial condition biases on the subsequent coupled simulation.

The atmospheric component of NU-WRF is based on the WRF model, a non-hydrostatic, compressible mesoscale model. In our configuration, we employ several key physics schemes to represent atmospheric processes. For cloud microphysics, we use the Thompson microphysics scheme (Thompson et al. 2008) which explicitly simulates the formation and evolution of various hydrometeors (e.g., cloud water, rain, ice, snow) within the atmosphere. For radiation, we use the Rapid Radiative Transfer Model for GCMs (RRTMG) radiation scheme (Iacono et al. 2008), which calculates the transfer of solar and terrestrial radiation. Both schemes are critical factors influencing the partitioning of energy and simulating precipitation during the flash drought experiment. The MYNN2.5 planetary boundary layer (PBL) scheme is used to parameterize the vertical turbulent mixing of momentum, heat, and moisture in the atmosphere, solving a prognostic equation for turbulent kinetic energy (TKE) to determine eddy diffusivities (Nakanishi and Niino 2006, 2009; Olson et al. 2019). This combination of physics routines has performed well in previous studies of Southern Great Plains atmospheric dynamics (Squitieri and Gallus 2016).

In this study, the Noah-MP land surface model (Niu et al. 2011; Yang et al. 2011) within LIS is configured with four soil layers and employs climatological MODIS green vegetation fraction (GVF) data in one experiment and GVF data that includes interannual variability (Nie et al. 2018) in another, enabling us to assess the impact of dynamic vegetation representation on flash drought simulations. Both the climatological (CLIM) and interannually varying (IVAR) GVF datasets are based on MODIS NDVI composites at a 0.05° spatial resolution from January 2002 to present (Nie et al. 2018) using the GVF estimation algorithm of Case et al. (2014). This dataset captures the unique interannual variability of vegetation health and cover, including the observed die-back and reduced greenness during the drought. We use the term "interannually-varying" to emphasize that the dataset reflects the specific year-to-year conditions of 2011, as opposed to a climatological seasonal cycle. Figure 2 shows the bi-weekly averaged difference in GVF between IVAR and CLIM for eight analysis boxes. As indicated in the figure, IVAR generally has lower GVF than CLIM during the study period, ranging up to a 25% drop in vegetation fraction.

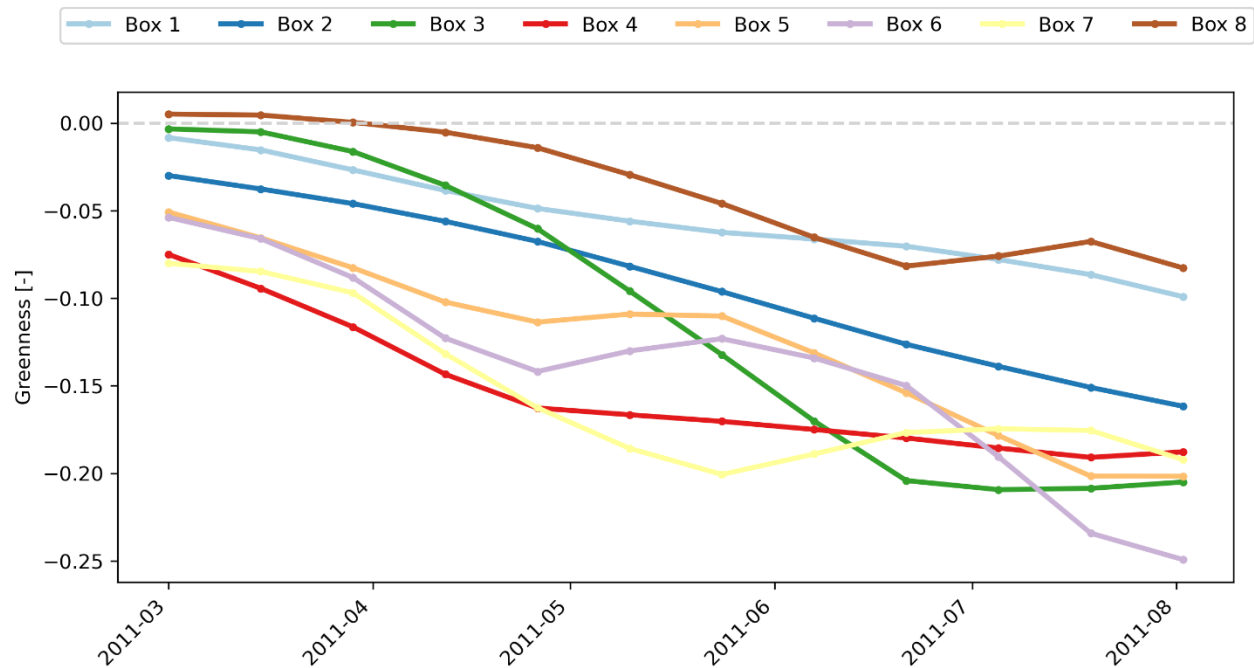


Figure 2: Difference in bi-weekly averaged Green Vegetation Fraction (GVF) between the interannually-varying vegetation experiment (IVAR) and the climatological vegetation experiment (CLIM; the 2001-2017 average) for the eight analysis boxes. Colors correspond to the analysis box colors in Figure 1. A negative difference indicates that the IVAR experiment shows lower GVF, as prescribed from observations, compared to the CLIM experiment.

In addition to the coupled NU-WRF simulations, we perform offline LIS simulations using the same implementation of Noah-MP. This allows us to compare representation of surface conditions during the drought in coupled and uncoupled simulations. For the offline simulations, the primary meteorological forcing for the simulations is derived from the MERRA-2 reanalysis data. However, to improve the representation of precipitation, the Integrated Multi-satellite Retrievals (IMERG) for NASA Global Precipitation Measurement (GPM) - GPM IMERG - precipitation data (Huffman et al. 2020) is used to replace the MERRA-2 precipitation forcing, as it offers high-resolution precipitation estimates that merge data from multiple satellite platforms and ground-based observations. In addition to providing a set of offline comparison simulations during the study period, this implementation of LIS provided surface initial conditions for the NU-WRF

simulations. All offline simulations used in the simulation were spun up for 40 years prior to the start of the study period to allow model soil moisture to reach equilibrium.

Results and Discussion

Observations of the 2011 drought

The 2011 Texas flash drought manifested as a complex interplay of meteorological and land-surface conditions, leading to rapid intensification and severe impacts across the Southern Great Plains. As illustrated in Figure 3, NLDAS-2 2m temperature and 10m wind speed (Xia et al. 2012) (anomalies were calculated relative to a climatology period of 1979-2020), ALEXI evapotranspiration (Anderson et al. 1997, 2007a,b) (anomalies were calculated relative to a climatology period of 2001-2021), MODIS SSEBoP evapotranspiration (Senay et al. 2011, 2013) (anomalies were calculated relative to a climatology period of 2000-2021), SMERGE root zone soil moisture (Tobin et al. 2019) (anomalies were calculated relative to a climatology period of 1979-2016) and CHIRPS precipitation data (Funk et al. 2015) (anomalies were calculated relative to a climatology period of 1981-2023) reveal key characteristics of this event and its evolution within the study domain. We have chosen these specific high-resolution observational products because they offer a more detailed and accurate representation of regional land-atmosphere processes compared to the MERRA-2 reanalysis ($\sim 0.5^\circ$), and they provide an independent and rigorous basis for model evaluation.

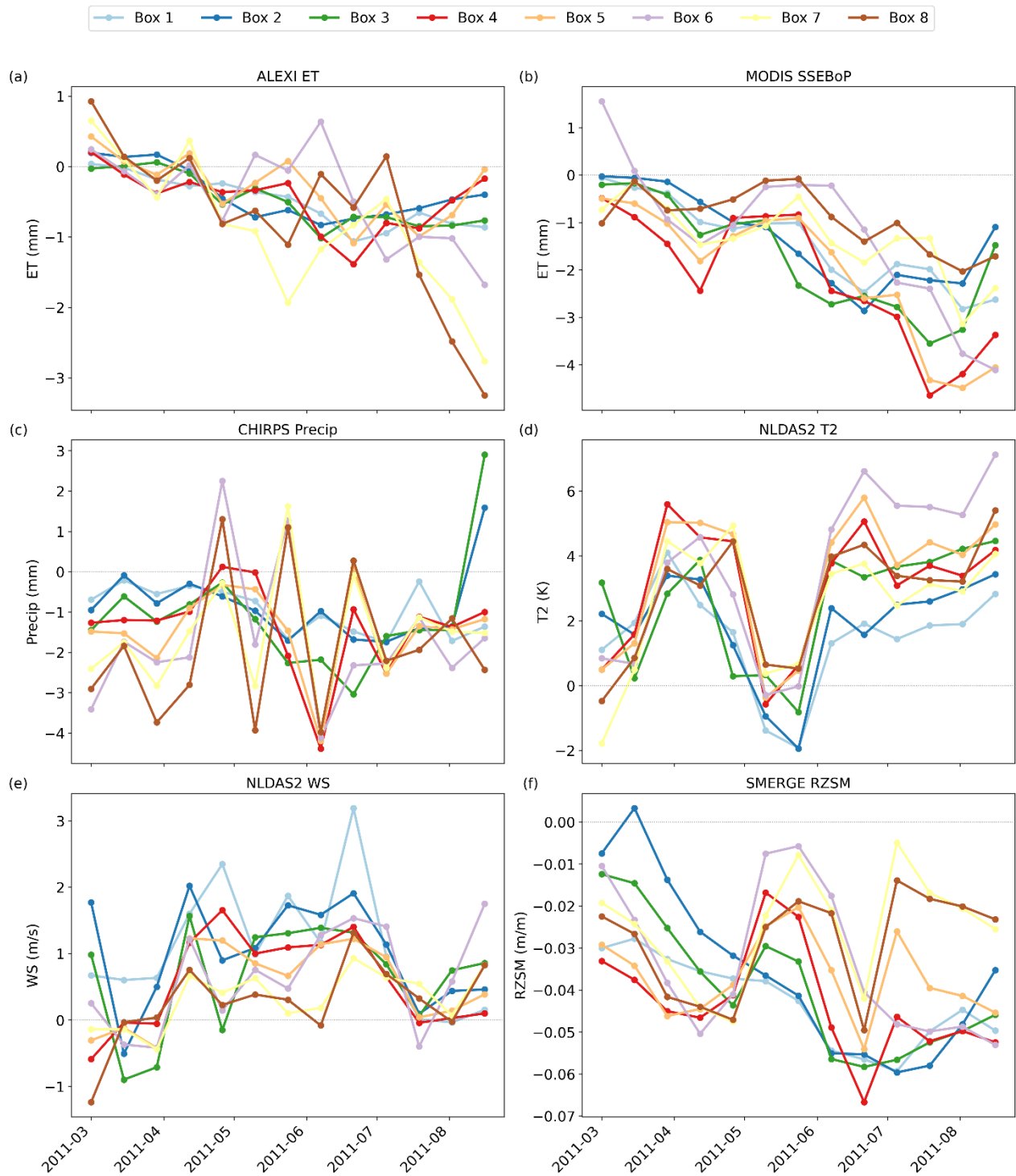


Figure 3: Difference in bi-weekly averaged observed atmospheric and land surface anomaly conditions during the study period from March 1st to August 1st compared to the long-term climatology for the used datasets of each plot. Note that the climatology periods vary depending on data availability.

The plot of 2m temperature anomalies (Figure 3-d) highlights the dramatic warming trend during the spring and summer of 2011. Positive anomalies began to emerge in April, with peak anomalies exceeding 6°C in some boxes. Conditions in May were mixed, with an average of two weeks relief from the observed abnormally hot conditions, though still warmer than average over the month. From late May onward anomalous warmth persisted throughout the summer, contributing to increased evaporative demand and exacerbating drought conditions. It is important to note that while these temperature anomalies suggest that dry conditions were present from early in the year, flash drought is specifically defined by the rapid decline in RZSM. Anomalously high temperatures, winds, and precipitation deficits can be contributing factors to flash drought (Otkin et al. 2018; Osman et al. 2022a; Chen et al. 2019), but the key characteristic is the rapid root zone soil moisture loss. Furthermore, there can be multiple flash drought episodes within a year if there are temporary recoveries in soil moisture (Osman et al., 2024). In this analysis, we are primarily focused on the most intense, widespread flash drought event that occurred during the summer months.

The climatology of evapotranspiration (ET) exhibits a typical seasonal pattern, with values increasing from spring to summer (Figure 4). However, the 2011 actual ET curves (Figures 3-a & 3-b) deviate significantly from this expected trend. Despite some slightly positive anomalies in early spring, a sharp decline in ET emerges from May onwards, coinciding with the onset of the flash drought. This decline reflects the vegetation's response to rapidly depleting soil moisture and increasing atmospheric demand, ultimately reducing evapotranspiration rates. Notably, these two diagnostic satellite products show no consistent evidence of enhanced springtime ET, a characteristic sometimes associated with flash droughts. ALEXI has some indication of an ET bump in early March, but it quickly fades, and MODIS SSEBoP doesn't show any at all. The observed ET decline in late spring aligns with the period of rapid warming and precipitation deficits, reinforcing the notion that land-atmosphere feedbacks, potentially modulated by vegetation, may play a meaningful role during drought intensification (Seneviratne et al. 2010; Miralles et al. 2019; Osman et al. 2022b).

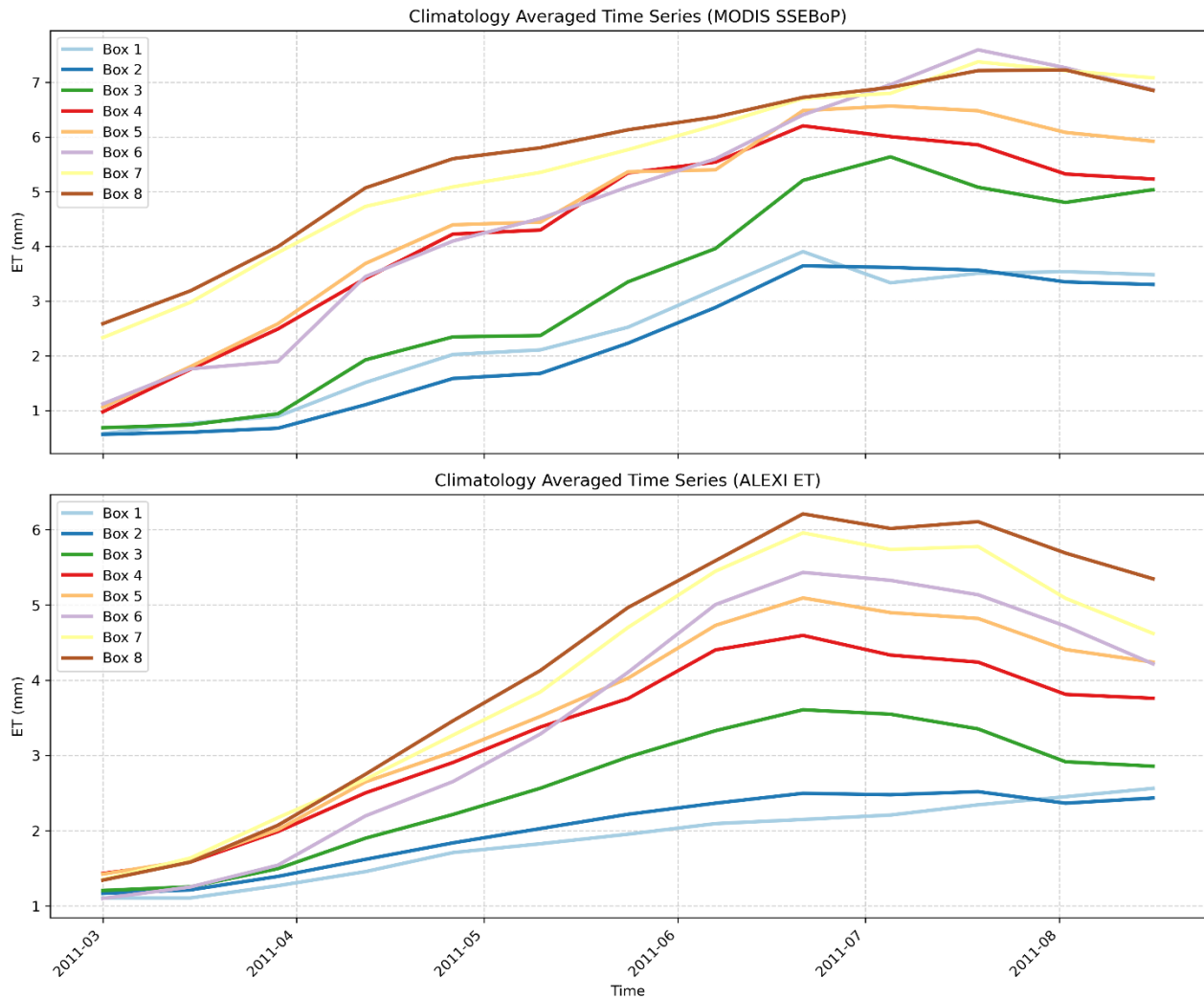


Figure 4: Climatological bi-weekly averaged observed evapotranspiration derived from MODIS SSEBoP (Top) and ALEXI (Bottom) datasets during the study period from March 1st to August 1st for the highlighted analysis boxes.

In the context of our flash drought analysis, bi-weekly averaged precipitation anomalies for the 2011 flash drought, derived from the Climate Hazards Group InfraRed Precipitation with Station data (CHIRPS) dataset for the period 1981-2021 (Figure 3-c), reveal a mixed pattern across the study area. While some regions experienced persistent precipitation deficits throughout the March-August period, others showed alternating periods of both deficit and surplus, highlighting the heterogeneous nature of flash drought processes (Osman et al. 2021, 2022a).

The flash drought onset dates for each of the eight study regions, derived from the Soil Moisture Volatility Index (SMVI) analysis presented in Osman et al. (2024) and illustrated in Figure 1, spanned from mid-May to early June. While the SMVI analysis may identify multiple flash drought episodes throughout the year, we primarily focus on the most intense, widespread events that occurred during the summer months, as these have the most significant impact. This timing coincides with observed anomalies in key hydrometeorological variables, including temperature, evapotranspiration, precipitation, and root-zone soil moisture (Figure 3). The rapid intensification of drought conditions, characterized by sharp declines in soil moisture, evapotranspiration, and mixed precipitation signals, underscores the "flashiness" of this event and its potential for severe impacts. It is notable that the diagnosed rapidity of onset results, to some extent, from the modest recovery period in early May: soil moisture deficits were flat or somewhat reduced between late April and the third week of May, before increasing quickly and dramatically during the period of diagnosed flash drought onset.

NU-WRF Simulations

To validate our experimental design, as shown in Figure 5, simulated evapotranspiration (ET) against observations, illustrating a key analogy: the deviation of the observed 2011 ALEXI data from its long-term climatology is analogous to the deviation of the IVAR simulation from the CLIM simulation. Specifically, the observed 2011 data shows a significant negative departure from its climatology, which is the signature of the drought's impact on ET. The IVAR simulation successfully reproduces this relative behavior, showing a similar downturn when compared to its corresponding baseline, the CLIM simulation. This demonstrates that while the model's absolute values have a notable bias, the inclusion of the drought-stressed Green Vegetation Fraction in the IVAR run induces a drought response that is consistent with observations. This validates our use of the IVAR-CLIM difference as a robust method for isolating the impacts of vegetation stress.

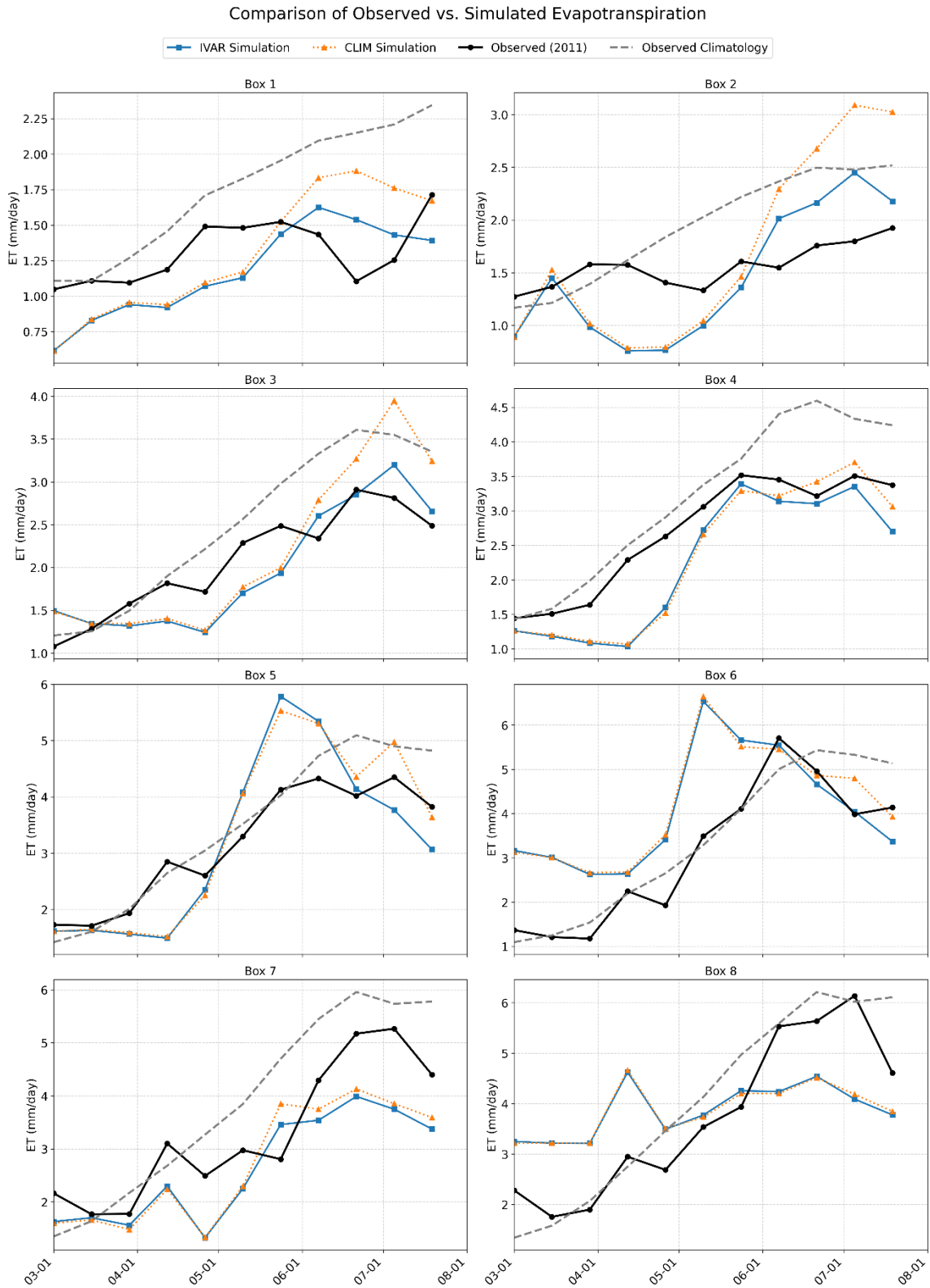


Figure 5. Comparison of bi-weekly averaged Evapotranspiration (ET) for each of the eight analysis boxes. The plot shows the observed ET during the 2011 event (solid black line), the long-

term observed climatology (dashed gray line), the simulation using interannually-varying vegetation for 2011 (IVAR, solid blue line), and the simulation using climatological vegetation (CLIM, dotted orange line).

We now turn to our simulation results, focusing on differences between the interannually-varying vegetation simulation (IVAR) and the climatological vegetation simulation (CLIM) in coupled NU-WRF runs. First, we examine what impact IVAR has on near-surface meteorology relative to the CLIM simulation. Across most boxes and time periods, we observe positive 2-m air temperature differences between simulations (IVAR - CLIM), indicating that the IVAR experiment, which incorporates real-time vegetation information, generally simulates higher 2m temperatures (T2) compared to the CLIM experiment (Figure 6a). This difference grows as the drought reaches maturity, but it is present to some extent throughout the simulation period. Impacts on precipitation are mixed (Figure 6b), as heterogeneity and mesoscale variability in land-atmosphere interactions lead to localization of precipitation anomalies as opposed to region-wide decreases in rainfall during the pre-drought and onset period.

Wind speeds tend to be higher (WS; Figure 6c), albeit by a modest amount in IVAR relative to CLIM, reflecting greater mixing in the planetary boundary layer, while near-surface specific humidity (Q2; Figure 6d) is substantially lower. This reduction in Q2, together with the increase in T2, indicates lower relative humidity and increased vapor pressure deficit (VPD; Figure 6h). IVAR also exhibits a deepened planetary boundary layer height (PBLH; Figure 6f) over time, as a product of increased turbulence associated with higher surface temperatures and Bowen ratios (sensible heat in favor of latent heat flux). There is some weaker expression of this in the mid-troposphere, as 500 hPa geopotential height tends to be elevated in IVAR relative to CLIM (GPH; Figure 5g).

It is tempting to compare plots of the difference between IVAR and CLIM simulations (like Figure 5) to observed anomalies, as shown in Figure 3. But the two are not actually comparable. Where observed anomalies show how 2011 differs from the average year, which could result from any number of large-scale to local climate processes, comparisons of IVAR to CLIM show only the simulated influence that anomalously low vegetation has on meteorological and hydrological conditions. Figure 5a, for example, shows a consistent but modest warming influence on

temperature that increases as the drought merges and matures. According to NLDAS (Figure 3d), temperature anomalies were substantially larger, and they did not show a systematic increase during the drought. The two results are not necessarily inconsistent; the counterfactual represented by the CLIM simulation (normal vegetation conditions under 2011 large-scale meteorology) is not directly observable.

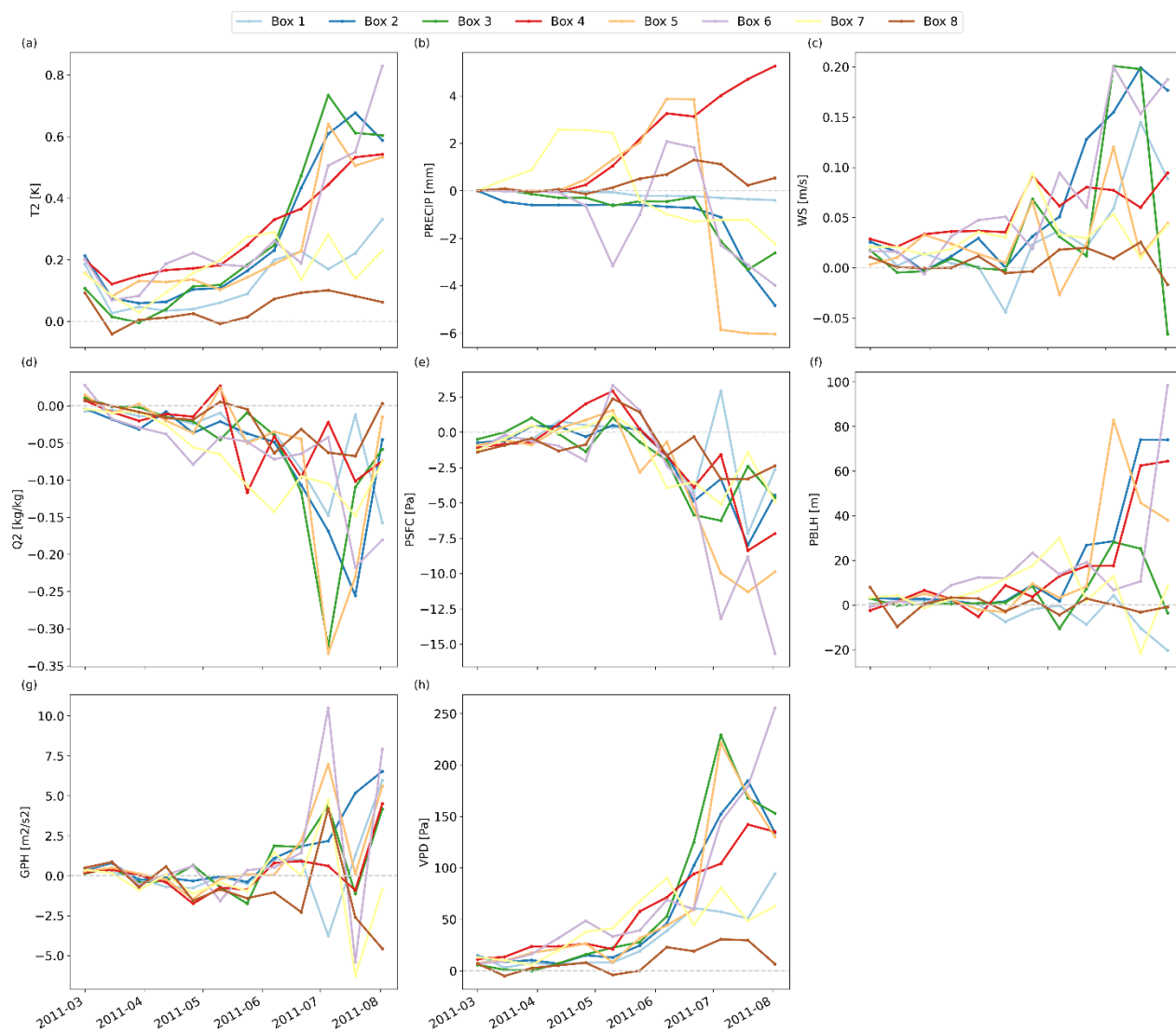


Figure 6: Bi-weekly averaged difference in near-surface meteorological fields between simulations using time-varying vegetation (IVAR) and climatological vegetation (CLIM) for the eight analysis boxes in the study area. All results shown are from the coupled NU-WRF simulations. (a) 2-meter

air temperature (T2), (b) Precipitation (PRECIP), (c) 10-meter wind speed (WS), (d) Water vapor mixing ratio at 2m (Q2), (e) Surface pressure (PSFC), (f) Planetary boundary layer height (PBLH), (g) Geopotential height at 500 hPa (GPH) and (h) Vapor pressure deficit (VPD).

Turning to the surface energy budget, we see that accounting for vegetation impacts of the drought in IVAR leads to a decrease in net radiation at the surface relative to CLIM (Figure 7a). This reduction is primarily attributable to higher surface temperatures (Figure 7b) that lead to increased upwelling longwave radiation from the surface (Figure 7c) associated with the warmer surface in IVAR simulations, and which is not fully compensated by increased downwelling longwave radiation (Figure 7d), resulting in a decrease in net longwave radiation at the surface (Figure 7e). The net shortwave radiation signal is mixed (Figure 7f) and is dominated by spatial variability in downwelling shortwave radiation (Figure 7g). There is a tendency towards increased reflected solar radiation (Figure 7h), but the reason for this is spatially variable: in some areas it is simply a product of increased downwelling shortwave radiation, while in others it is a result of drought-induced brightening of the surface (Zaitchik et al. 2013) – a phenomenon that was patchy during this event and mostly emerged later in drought development.



Figure 7: Weekly averaged difference in radiation balance fields between simulations using interannually-varying vegetation (IVAR) and climatological vegetation (CLIM) for the eight analysis boxes in the study area. (a) Net radiation balance (R_{net}), (b) Surface temperature (T_s), (c) upward longwave radiation at the surface ($LWUPB$), (d) downward longwave radiation at the surface ($LWDNB$), (e) net longwave radiation ($LWNET$), (f) net shortwave radiation ($SWNET$), (g) downward shortwave radiation at the surface ($SWDNB$), and (h) upward shortwave radiation at the surface ($SWUPB$).

The drought also significantly alters turbulent energy fluxes, as evidenced by the pronounced reduction in latent heat flux (i.e. evapotranspiration) (Figure 8a) and mixed signals (with an overall slight reduction trend) in sensible heat flux (Figure 8b). This altered energy partitioning is

consistent with satellite-derived observations and with the simulated reduction in net radiation at the surface (Figure 7a) and with a situation of water limitation: vapor pressure deficit and potential evapotranspiration are increased, but accounting for vegetation die-back in IVAR reduces simulated plant access to deeper soil moisture reserves, such that actual evapotranspiration (or latent heat flux) is reduced. Both the latent and the sensible heat flux difference develop primarily after drought initiation, indicating that the simulations do not show a strong role of vegetation-mediated suppression of latent or sensible heat flux during the onset of flash drought. The latent and sensible heat flux results are also consistent with previous studies that have highlighted the potential for drought to lead to reduced net radiation and lower energy conditions near the surface (Osman et al. 2022b; Miralles et al. 2019).

Taken together, these results illustrate a self-intensifying feedback loop in WRF simulations that is driven by vegetation stress, as conceptualized in Figure 9. The prescribed reduction in green vegetation fraction in the IVAR simulation directly curtails evapotranspiration, reducing the latent heat flux (LH) by over 10 W/m^2 in some regions during the peak drought (Figure 8a). This partitions more energy into the sensible heat flux (HFX), increasing the Bowen ratio and leading to a warmer land surface and overlying atmosphere, with 2-meter air temperatures increasing by up to 0.8 K (Figure 6a). The warmer, drier boundary layer, which also deepens significantly (Figure 6f), results in a substantial increase in the vapor pressure deficit (VPD) by over 200 Pa in some boxes (Figure 6h). This heightened atmospheric demand for moisture further stresses the remaining vegetation, creating a positive feedback that amplifies meteorological drought conditions.

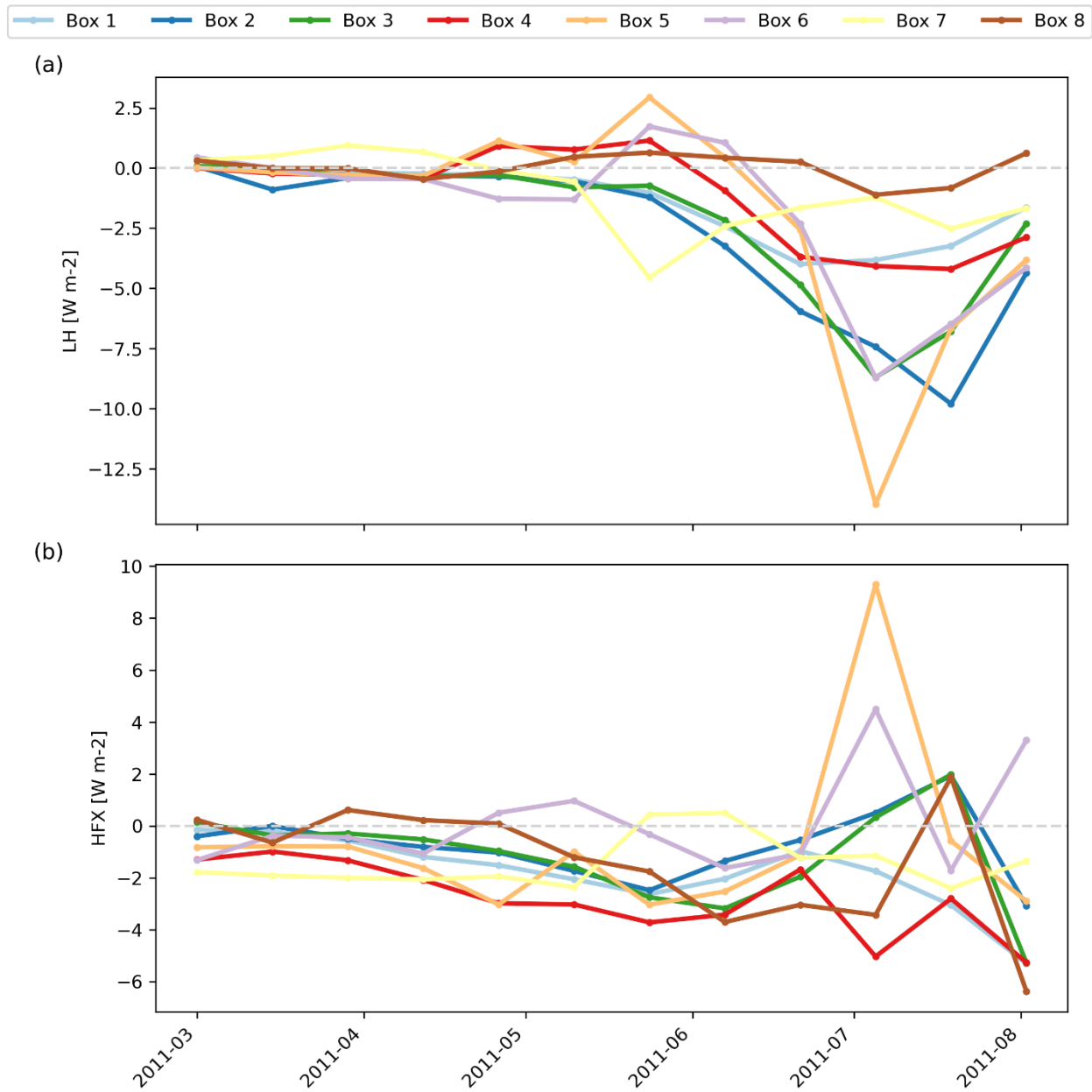


Figure 8: Biweekly averaged difference in turbulent energy fluxes between simulations using interannually-varying vegetation (IVAR) and climatological vegetation (CLIM) for the eight analysis boxes in the study area. (a) Latent heat flux (LH), (b) Sensible heat flux (HFX).

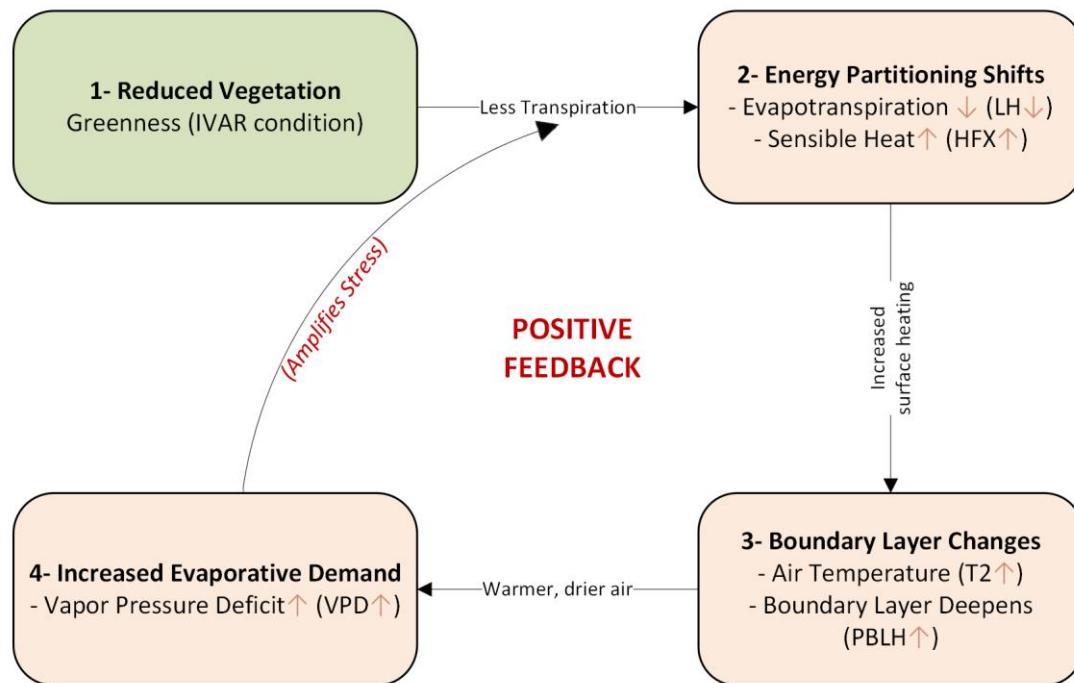


Figure 9: Schematic of the vegetation-mediated positive feedback loop that amplifies flash drought conditions in WRF simulations. The process is initiated by (1) an observed reduction in green vegetation cover. This leads to (2) a shift in surface energy partitioning away from latent heat and toward sensible heat, which in turn (3) warms and deepens the planetary boundary layer. The resulting (4) increase in vapor pressure deficit enhances atmospheric evaporative demand, creating a reinforcing feedback that further stresses vegetation and intensifies the drought.

While the surface radiation and energy partitioning results are consistent with each other, it is interesting that the PBL is deeper in IVAR, particularly as the drought reaches maturity, even though surface turbulent energy fluxes are reduced. To explore this result, we examine atmospheric turbulence, as captured by turbulent kinetic energy (TKE) profiles. The vertical profiles of TKE differences between the IVAR and CLIM experiments (Figure 10) reveal how vegetation alters turbulence throughout the planetary boundary layer. Positive values indicate increased TKE in the IVAR experiment, suggesting that under drought stress, atmospheric turbulence is enhanced. The pattern extends as high as ~5km above the surface (approximately the 40th vertical model level). This is somewhat counterintuitive, given the reduction in surface turbulent energy fluxes (sensible and latent heat flux) in IVAR relative to CLIM. However, both longwave radiative heating of the boundary layer from the surface and regionally warmer

conditions in the IVAR simulation could contribute to higher PBL temperatures and greater TKE. It's also important to consider that larger-scale atmospheric feedbacks, particularly during heatwaves, may play a significant role. For example, the PBLH can more easily grow into a warm, dry entrainment zone, especially over multiple days as conditions become drier and warmer. In such situations, the PBL preconditions itself for rapid growth due to the residual layer, potentially reducing the direct influence of surface forcing on TKE. Even if these processes are not fully captured in turbulent energy fluxes between the surface and the lowest model layer, they can still significantly influence TKE.

The spatial and temporal variability in TKE differences suggests that the influence of drought conditions on atmospheric turbulence is most pronounced in transitional zones (Boxes 2-7) with moderate vegetation cover, while it is less evident in both the most humid (Box 8) and most arid (Box 1) regions. This is consistent with the spatial pattern of IVAR vs. CLIM differences in several other fields (e.g., T2, Ts, LH) which also show largest impacts in the transitional zone between humid areas with dense and deeply rooted vegetation (Box 8) and sparse vegetation in arid regions (Box 1).

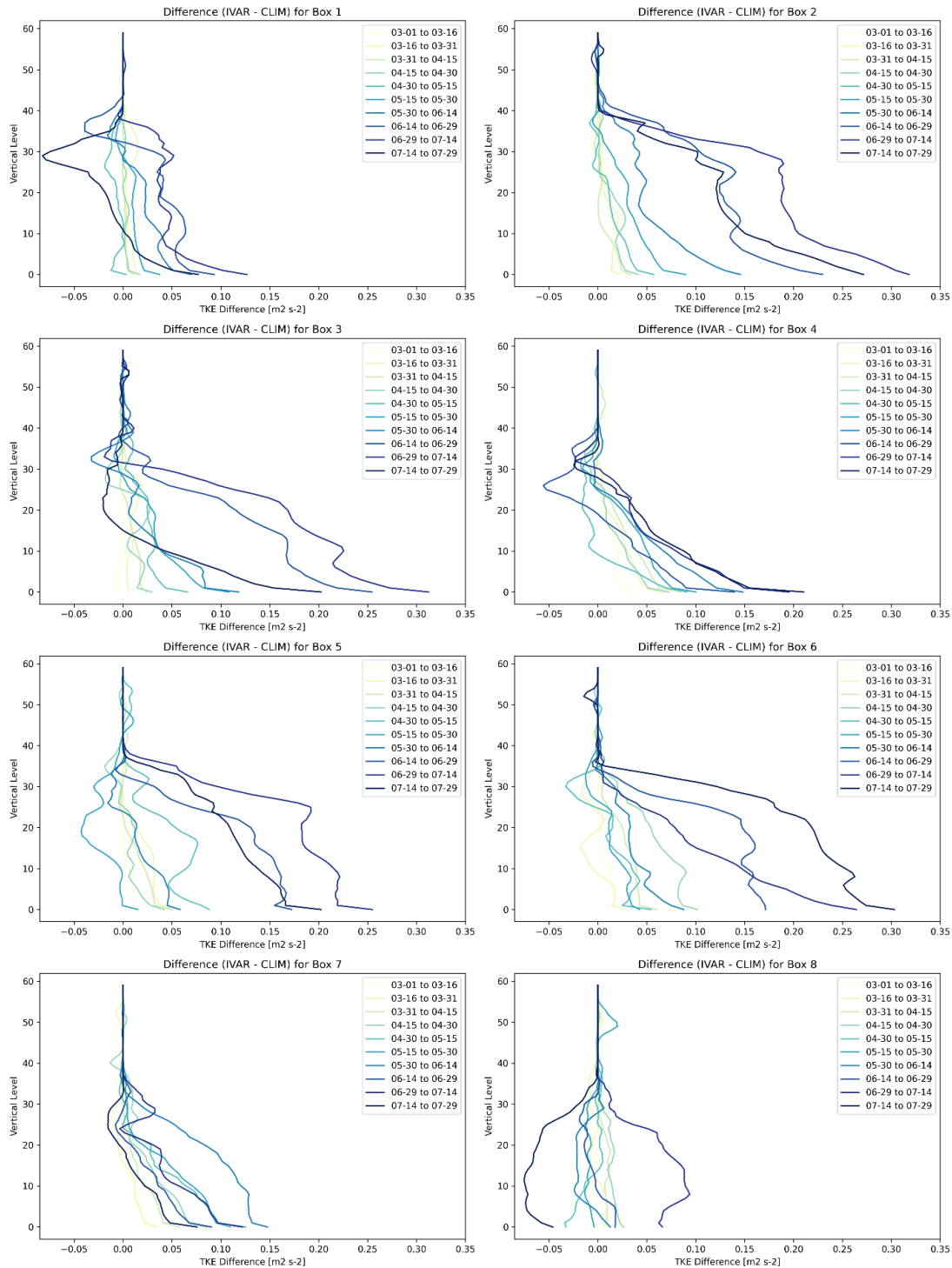


Figure 10: Vertical profiles of differences in the turbulent kinetic energy (TKE) from the MYNN2.5 planetary boundary layer scheme between the IVAR and CLIM experiments for the eight selected boxes in the Southern Great Plains averaged over 2-week time periods during the 2011 flash drought.

Regional Differences in Land-Atmosphere Feedbacks

As noted in the figures, the impact of accounting for vegetation anomalies is not uniform across the study domain. The differences between the IVAR and CLIM simulations show clear spatial and temporal variability that can be linked to the underlying vegetation characteristics of each analysis box. The most pronounced vegetation-mediated feedbacks—as seen in the largest differences in 2-meter temperature (Figure 5a), latent heat flux (Figure 7a), and vapor pressure deficit (Figure 5h)—tend to occur in the transitional zones (Boxes 2-7). These regions, characterized by savannas, grasslands, and croplands with moderate vegetation cover, are highly susceptible to strong land-atmosphere coupling. In these areas, the vegetation's response to water stress, such as stomatal closure and reduced evapotranspiration, has a more significant impact on the surface energy budget and, consequently, the overlying atmosphere.

In contrast, the simulated differences are less pronounced in the more arid (Box 1) and most humid (Box 8) regions. In the arid box, vegetation is already sparse, so the difference between climatological and interannually-varying greenness is less impactful on a larger scale. In the humid box, dense, deeply-rooted vegetation may have access to a more stable soil moisture supply, making it more resilient to short-term precipitation deficits and leading to a more muted land-atmosphere feedback signal. These regional variations provide a novel insight into the localized nature of flash drought intensification and highlight the importance of not only representing vegetation variability but also considering the specific hydroclimatic regime in which these feedbacks occur.

Coupled vs. Offline Simulations

We have focused on results from our coupled land-atmosphere simulations. However, as noted in the methods section, we also conducted offline simulations in which the drought period was simulated with Noah-MP using prescribed meteorological forcing. This comparison was done to isolate the impact of two-way land-atmosphere feedbacks—such as when a reduction in surface moisture heats the overlying atmosphere, which in turn increases evaporative demand and further dries the land surface. The key question was whether these feedback loops, which are absent in the offline runs, amplify or dampen the effect of vegetation anomalies seen in the IVAR versus CLIM experiments.

The results reveal that the feedbacks substantially amplify the differences between the IVAR and CLIM simulations. This amplification is evident in the surface energy budget. For instance, the initial reduction in latent heat flux (LH) in the coupled IVAR run (due to vegetation stress) led to warmer and drier near-surface atmospheric conditions. This atmospheric response, which cannot occur in the offline run, created higher evaporative demand that further suppressed LH. As a result, the total reduction in LH within the IVAR simulation relative to the CLIM simulation was significantly more pronounced in the coupled run than it was in the offline-only comparison. Concurrently, the partitioning of energy into sensible heat flux (HFX) was also magnified. During peak drought intensification, these feedback-driven processes were found to alter the IVAR-CLIM difference in surface fluxes by more than 30% compared to what was seen in the offline simulation.

This analysis demonstrates that two-way feedbacks are not a minor effect, but rather a critical mechanism that magnifies the impact of vegetation stress on the surface energy budget and atmospheric boundary layer. It confirms that the land surface does not merely respond to the atmosphere, but actively shapes it during drought evolution. Therefore, the use of a fully coupled modeling system is essential to capturing the self-intensifying nature of flash droughts and understanding the full effect of vegetation's role.

Conclusion

The 2011 Texas flash drought, a landmark event in its intensity and widespread impacts, occurred in a region hypothesized to have strong land-atmosphere coupling (Koster et al. 2004). Here, we have investigated whether vegetation-mediated land-atmosphere feedbacks might have played an important role in the drought's onset and development. In observation and controlled numerical experiment, we find that the drought exhibits some but not all of the dynamics that have been invoked in studies of flash drought process. The event does not, in remote sensing data or simulation, show a strong pre-drought enhancement in ET. So, for this event, it does not appear that early green-up and vegetation-driven soil moisture depletion played a major role in priming the surface for drought. Once the drought began, however, we see that accounting for drought impacts in vegetation—our IVAR simulation—results in reduced net radiation, lower turbulent heat flux, higher vapor pressure deficit, and increased evaporative demand relative to a simulation

(CLIM) that does not account for these vegetation impacts. This suggests that, at least within our modeling framework, vegetation feedbacks act to intensify meteorological conditions that lead to vegetation stress.

Importantly, the strength of this feedback is not uniform; it was most pronounced in the transitional, semi-arid regions of our study domain and more muted in the most arid and humid zones, highlighting that the background hydroclimate strongly modulates the role of vegetation in drought intensification. These simulation results point to the potential value in of including drought-induced vegetation dynamics in dynamically-based simulation and forecasting systems. In this study we prescribed vegetation conditions based on observations, but in a forecast context one would need to include a dynamic phenology model to capture these anomalies. In pointing to this potential, we acknowledge that limited observations and the fact that we were not able to perform extended multi-year NU-WRF simulations limit our ability to quantify the performance of IVAR relative to CLIM in a statistical significance sense. Rather, our purely descriptive conclusions are drawn from the fact that differences between IVAR and CLIM are substantial and, in the case of observable variables, tend to be of the same sign as the anomalies observed during the drought event.

It is important to contextualize these findings within the hydroclimate of the Southern Great Plains, a region known to be a "hotspot" for strong land-atmosphere coupling. The significant feedback signal we observed is likely amplified in this transitional, water-limited environment where evapotranspiration is highly sensitive to vegetation health and soil moisture. In other regions, such as energy-limited humid climates or heavily irrigated agricultural basins, the vegetation-mediated feedbacks observed here might be muted or fundamentally different. For instance, in energy-limited systems, reductions in vegetation may not lead to the same degree of surface warming, while access to deep soil moisture or irrigation could decouple vegetation from short-term precipitation deficits. Therefore, while our results underscore the critical importance of vegetation dynamics, the specific nature of the feedback loop is likely dependent on the regional climatic and land-use regime.

Further research is required to explore the role of specific vegetation types and their physiological responses to drought stress in modulating land-atmosphere feedbacks. From a prediction

standpoint, data assimilation (DA) offers a promising avenue for addressing the challenges of incorporating these complex vegetation dynamics. The integration of additional observational data, such as soil moisture and vegetation indices, through DA techniques, may enhance model performance and capture the full spectrum of flash drought dynamics in real-time forecasting. This approach could potentially reduce the reliance on dynamic vegetation models, which are still a work in progress and face significant uncertainties in accurately representing vegetation behavior. The insights gained from this study serve as a steppingstone towards a more comprehensive and predictive understanding of flash droughts.

Acknowledgement

This research was made possible by funding from the NASA ROSES program. The authors wish to express their gratitude to the Department of Earth and Planetary Sciences at Johns Hopkins University for providing resources and support. We also extend our sincere appreciation to the peer reviewers and our collaborators for their insightful feedback and contributions that significantly improved the quality of this work.

Availability Statement

The numerical model simulations upon which this study is based are too large to archive or to transfer. Instead, we provide all the information needed to replicate the simulations; we used NU-WRF model version 11.2 (acquiring the model is subject to NASA legal review and requires users to sign the software agreement - <https://nuwrf.gsfc.nasa.gov/software>). The model configuration files and namelist settings are publicly published by Osman 2025 under DOI:[10.17632/f4zxxscrkg.1](https://doi.org/10.17632/f4zxxscrkg.1).

References

- Adhikari, S., W. Zhou, Z. Dou, N. Sakib, R. Ma, B. Chaudhari, and B. Liu, 2024: Analysis of Flash Drought and Its Impact on Forest Normalized Difference Vegetation Index (NDVI) in Northeast China from 2000 to 2020. *Atmosphere*, **15**, 818, <https://doi.org/10.3390/atmos15070818>.
- Ahmad, S. K., and Coauthors, 2022: Flash Drought Onset and Development Mechanisms Captured With Soil Moisture and Vegetation Data Assimilation. *Water Resour. Res.*, **58**, 1–17, <https://doi.org/10.1029/2022WR032894>.
- Anderson, M. C., J. M. Norman, G. R. Diak, W. P. Kustas, and J. R. Mecikalski, 1997: A two-source time-integrated model for estimating surface fluxes using thermal infrared remote sensing. *Remote Sens. Environ.*, **60**, 195–216, [https://doi.org/10.1016/S0034-4257\(96\)00215-5](https://doi.org/10.1016/S0034-4257(96)00215-5).
- Anderson, M. C., J. M. Norman, J. R. Mecikalski, J. A. Otkin, and W. P. Kustas, 2007a: A climatological study of evapotranspiration and moisture stress across the continental United States based on thermal remote sensing: 1. Model formulation. *J. Geophys. Res. Atmospheres*, **112**, 2006JD007506, <https://doi.org/10.1029/2006jd007506>.
- , ———, ———, ———, and ———, 2007b: A climatological study of evapotranspiration and moisture stress across the continental United States based on thermal remote sensing: 2. Surface moisture climatology. *J. Geophys. Res. Atmospheres*, **112**, D11112, <https://doi.org/10.1029/2006JD007507>.
- Arsenault, K. R., G. S. Nearing, S. Wang, S. Yatheendradas, and C. D. Peters-Lidard, 2018: Parameter sensitivity of the Noah-MP land surface model with dynamic vegetation. *J. Hydrometeorol.*, **19**, 815–830, <https://doi.org/10.1175/JHM-D-17-0205.1>.
- Basara, J. B., and J. I. Christian, 2018: Seasonal and interannual variability of land–atmosphere coupling across the Southern Great Plains of North America using the North American regional reanalysis. *Int. J. Climatol.*, **38**, 964–978, <https://doi.org/10.1002/joc.5223>.

- Case, J. L., F. J. LaFontaine, J. R. Bell, G. J. Jedlovec, S. V. Kumar, and C. D. Peters-Lidard, 2014: A Real-Time MODIS Vegetation Product for Land Surface and Numerical Weather Prediction Models. *IEEE Trans. Geosci. Remote Sens.*, **52**, 1772–1786, <https://doi.org/10.1109/TGRS.2013.2255059>.
- Chen, L. G., J. Gottschalck, A. Hartman, D. Miskus, R. Tinker, and A. Artusa, 2019: Flash Drought Characteristics Based on U.S. Drought Monitor. *Atmosphere*, **10**, 498, <https://doi.org/10.3390/atmos10090498>.
- Chiang, F., O. Mazdiyasi, and A. AghaKouchak, 2018: Amplified warming of droughts in southern United States in observations and model simulations. *Sci. Adv.*, **4**, eaat2380, <https://doi.org/10.1126/sciadv.aat2380>.
- Dirmeyer, P. A., 2011: The terrestrial segment of soil moisture-climate coupling: SOIL MOISTURE-CLIMATE COUPLING. *Geophys. Res. Lett.*, **38**, n/a-n/a, <https://doi.org/10.1029/2011GL048268>.
- Entekhabi, D., 2023: Propagation in the Drought Cascade: Observational Analysis Over the Continental US. *Water Resour. Res.*, **59**, e2022WR032608, <https://doi.org/10.1029/2022WR032608>.
- Fallah, A., M. A. Barlow, L. Agel, J. Kim, J. Mankin, D. M. Mocko, and C. B. Skinner, 2024: Impact of Vegetation Assimilation on Flash Drought Characteristics across the Continental United States. *J. Hydrometeorol.*, **25**, 1263–1281, <https://doi.org/10.1175/JHM-D-23-0219.1>.
- Funk, C., and Coauthors, 2015: The climate hazards infrared precipitation with stations—a new environmental record for monitoring extremes. *Sci. Data*, **2**, 150066, <https://doi.org/10.1038/sdata.2015.66>.
- Gelaro, R., and Coauthors, 2017: The Modern-Era Retrospective Analysis for Research and Applications, Version 2 (MERRA-2). *J. Clim.*, **30**, 5419–5454, <https://doi.org/10.1175/JCLI-D-16-0758.1>.

- Huffman, G. J., and Coauthors, 2020: Integrated Multi-satellite Retrievals for the Global Precipitation Measurement (GPM) Mission (IMERG). *Satellite Precipitation Measurement: Volume 1*, V. Levizzani, C. Kidd, D.B. Kirschbaum, C.D. Kummerow, K. Nakamura, and F.J. Turk, Eds., Springer International Publishing, 343–353, https://doi.org/10.1007/978-3-030-24568-9_19.
- Iacono, M. J., J. S. Delamere, E. J. Mlawer, M. W. Shephard, S. A. Clough, and W. D. Collins, 2008: Radiative forcing by long-lived greenhouse gases: Calculations with the AER radiative transfer models. *J. Geophys. Res. Atmospheres*, **113**, 2008JD009944, <https://doi.org/10.1029/2008JD009944>.
- Jiang, Y., H. Shi, Z. Wen, X. Yang, Y. Wu, and L. Li, 2024: Monitoring of Flash Drought on the Loess Plateau and Its Impact on Vegetation Ecosystems, <https://doi.org/10.3390/f15081455>.
- Koster, R. D., and Coauthors, 2004: Regions of strong coupling between soil moisture and precipitation. *Science*, **305**, 1138–1140, <https://doi.org/10.1126/science.1100217>.
- Koster, R. D., S. D. Schubert, H. Wang, S. P. Mahanama, and A. M. Deangelis, 2019: Flash drought as captured by reanalysis data: Disentangling the contributions of precipitation deficit and excess evapotranspiration. *J. Hydrometeorol.*, **20**, 1241–1258, <https://doi.org/10.1175/JHM-D-18-0242.1>.
- Kumar, S. V., and Coauthors, 2006: Land information system: An interoperable framework for high resolution land surface modeling. *Environ. Model. Softw.*, **21**, 1402–1415, <https://doi.org/10.1016/J.ENVSOFT.2005.07.004>.
- Lawal, S., J. Costanza, F. H. Koch, and R. M. Scheller, 2024: Modeling the impacts of hot drought on forests in Texas. *Front. For. Glob. Change*, **7**, <https://doi.org/10.3389/ffgc.2024.1280254>.
- Osman, M, 2025: Role of Vegetation in Flash Drought using NU-WRF, *Mendeley Data*, *V1*, <https://doi.org/10.17632/f4zxxscrkg.1>

- Miralles, D. G., P. Gentine, S. I. Seneviratne, and A. J. Teuling, 2019: Land–atmospheric feedbacks during droughts and heatwaves: state of the science and current challenges. *Ann. N. Y. Acad. Sci.*, **1436**, 19–35, <https://doi.org/10.1111/nyas.13912>.
- Mocko, D. M., S. V. Kumar, C. D. Peters-Lidard, and S. Wang, 2021: Assimilation of vegetation conditions improves the representation of drought over agricultural areas. *J. Hydrometeorol.*, **22**, 1085–1098, <https://doi.org/10.1175/JHM-D-20-0065.1>.
- Nakanishi, M., and H. Niino, 2006: An Improved Mellor–Yamada Level-3 Model: Its Numerical Stability and Application to a Regional Prediction of Advection Fog. *Bound.-Layer Meteorol.*, **119**, 397–407, <https://doi.org/10.1007/s10546-005-9030-8>.
- , and ———, 2009: Development of an Improved Turbulence Closure Model for the Atmospheric Boundary Layer. *J. Meteorol. Soc. Jpn. Ser II*, **87**, 895–912, <https://doi.org/10.2151/jmsj.87.895>.
- Nie, W., B. F. Zaitchik, M. Rodell, S. V. Kumar, M. C. Anderson, and C. Hain, 2018: Groundwater Withdrawals Under Drought: Reconciling GRACE and Land Surface Models in the United States High Plains Aquifer. *Water Resour. Res.*, **54**, 5282–5299, <https://doi.org/10.1029/2017WR022178>.
- , and Coauthors, 2022: Towards effective drought monitoring in the Middle East and North Africa (MENA) region: implications from assimilating leaf area index and soil moisture into the Noah-MP land surface model for Morocco. *Hydrol. Earth Syst. Sci.*, **26**, 2365–2386, <https://doi.org/10.5194/hess-26-2365-2022>.
- Nielsen-Gammon, J., 2012: The 2011 Texas Drought. *Tex. Water J.*, **3**, 59–95, <https://doi.org/10.21423/twj.v3i1.6463>.
- Niu, G.-Y., and Coauthors, 2011: The community Noah land surface model with multiparameterization options (Noah-MP): 1. Model description and evaluation with local-scale measurements. *J. Geophys. Res.*, **116**, D12109, <https://doi.org/10.1029/2010JD015139>.

- Olson, J. B., J. S. Kenyon, Wayne. A. Angevine, J. M. Brown, M. Pagowski, and K. Sušelj, 2019: A Description of the MYNN-EDMF Scheme and the Coupling to Other Components in WRF–ARW, <https://doi.org/10.25923/N9WM-BE49>.
- Osman, M., B. F. Zaitchik, H. S. Badr, J. I. Christian, T. Tadesse, J. A. Otkin, and M. C. Anderson, 2021: Flash drought onset over the contiguous United States: sensitivity of inventories and trends to quantitative definitions. *Hydrol. Earth Syst. Sci.*, **25**, 565–581, <https://doi.org/10.5194/hess-25-565-2021>.
- , and Coauthors, 2022a: Diagnostic Classification of Flash Drought Events Reveals Distinct Classes of Forcings and Impacts. *J. Hydrometeorol.*, **23**, 275–289, <https://doi.org/10.1175/JHM-D-21-0134.1>.
- Osman, M., B. F. Zaitchik, and N. S. Winstead, 2022b: Cascading Drought-Heat Dynamics During the 2021 Southwest United States Heatwave. *Geophys. Res. Lett.*, **49**, e2022GL099265, <https://doi.org/10.1029/2022GL099265>.
- Osman, M., B. Zaitchik, J. Otkin, and M. Anderson, 2024: A global flash drought inventory based on soil moisture volatility. *Sci. Data*, **11**, 965, <https://doi.org/10.1038/s41597-024-03809-9>.
- Otkin, J. A., M. C. Anderson, C. Hain, I. E. Mladenova, J. B. Basara, and M. Svoboda, 2013: Examining Rapid Onset Drought Development Using the Thermal Infrared–Based Evaporative Stress Index. *J. Hydrometeorol.*, **14**, 1057–1074, <https://doi.org/10.1175/JHM-D-12-0144.1>.
- , M. Svoboda, E. D. Hunt, T. W. Ford, M. C. Anderson, C. Hain, and J. B. Basara, 2018: Flash Droughts: A Review and Assessment of the Challenges Imposed by Rapid-Onset Droughts in the United States. *Bull. Am. Meteorol. Soc.*, **99**, 911–919, <https://doi.org/10.1175/BAMS-D-17-0149.1>.
- Parazoo, N., M. Osman, M. Pascolini-Campbell, and B. Byrne, 2024: Antecedent Conditions Mitigate Carbon Loss During Flash Drought Events. *Geophys. Res. Lett.*, **51**, <https://doi.org/10.1029/2024GL108310>.

- Pendergrass, A. G., and Coauthors, 2020: Flash droughts present a new challenge for subseasonal-to-seasonal prediction. *Nat. Clim. Change*, **10**, 191–199, <https://doi.org/10.1038/s41558-020-0709-0>.
- Peters-Lidard, C. D., and Coauthors, 2007: High-performance Earth system modeling with NASA/GSFC's Land Information System. *Innov. Syst. Softw. Eng.*, **3**, 157–165, <https://doi.org/10.1007/s11334-007-0028-x>.
- , and Coauthors, 2015: Integrated modeling of aerosol, cloud, precipitation and land processes at satellite-resolved scales. *Environ. Model. Softw.*, **67**, 149–159, <https://doi.org/10.1016/j.envsoft.2015.01.007>.
- Schumacher, D. L., J. Keune, P. Dirmeyer, and D. G. Miralles, 2022: Drought self-propagation in drylands due to land–atmosphere feedbacks. *Nat. Geosci.* 2022, 1–7, <https://doi.org/10.1038/s41561-022-00912-7>.
- Schwantes, A. M., J. J. Swenson, and R. B. Jackson, 2016: Quantifying drought-induced tree mortality in the open canopy woodlands of central Texas. *Remote Sens. Environ.*, **181**, 54–64, <https://doi.org/10.1016/j.rse.2016.03.027>.
- Senay, G. B., M. E. Budde, and J. P. Verdin, 2011: Enhancing the Simplified Surface Energy Balance (SSEB) approach for estimating landscape ET: Validation with the METRIC model. *Agric. Water Manag.*, **98**, 606–618, <https://doi.org/10.1016/j.agwat.2010.10.014>.
- Senay, G. B., S. Bohms, R. K. Singh, P. H. Gowda, N. M. Velpuri, H. Alemu, and J. P. Verdin, 2013: Operational Evapotranspiration Mapping Using Remote Sensing and Weather Datasets: A New Parameterization for the SSEB Approach. *JAWRA J. Am. Water Resour. Assoc.*, **49**, 577–591, <https://doi.org/10.1111/JAWR.12057>.
- Seneviratne, S. I., T. Corti, E. L. Davin, M. Hirschi, E. B. Jaeger, I. Lehner, B. Orlowsky, and A. J. Teuling, 2010: Investigating soil moisture–climate interactions in a changing climate: A review. *Earth-Sci. Rev.*, **99**, 125–161, <https://doi.org/10.1016/j.earscirev.2010.02.004>.

- Skamarock, W. C., and Coauthors, 2021: A Description of the Advanced Research WRF Model Version 4.3. *NCAR Tech. Note*, **TN-556+STR**, 1–165, <https://doi.org/10.5065/1dfh-6p97>.
- Squitieri, B. J., and W. A. Gallus, 2016: WRF Forecasts of Great Plains Nocturnal Low-Level Jet-Driven MCSs. Part I: Correlation between Low-Level Jet Forecast Accuracy and MCS Precipitation Forecast Skill. *Weather Forecast.*, **31**, 1301–1323, <https://doi.org/10.1175/WAF-D-15-0151.1>.
- Svoboda, M., and Coauthors, 2002: The Drought Monitor. *Bull. Am. Meteorol. Soc.*, **83**, 1181–1190, <https://doi.org/10.1175/1520-0477-83.8.1181>.
- Tallaksen, L. M., and K. Stahl, 2014: Spatial and temporal patterns of large-scale droughts in Europe: Model dispersion and performance. *Geophys. Res. Lett.*, **41**, 429–434, <https://doi.org/10.1002/2013GL058573>.
- Thompson, G., P. R. Field, R. M. Rasmussen, and W. D. Hall, 2008: Explicit Forecasts of Winter Precipitation Using an Improved Bulk Microphysics Scheme. Part II: Implementation of a New Snow Parameterization. *Mon. Weather Rev.*, **136**, 5095–5115, <https://doi.org/10.1175/2008MWR2387.1>.
- Tobin, K. J., W. T. Crow, J. Dong, and M. E. Bennett, 2019: Validation of a New Root-Zone Soil Moisture Product: Soil MERGE. *IEEE J. Sel. Top. Appl. Earth Obs. Remote Sens.*, **12**, 3351–3365, <https://doi.org/10.1109/JSTARS.2019.2930946>.
- Ukkola, A. M., M. G. De Kauwe, A. J. Pitman, M. J. Best, G. Abramowitz, V. Haverd, M. Decker, and N. Haughton, 2016a: Land surface models systematically overestimate the intensity, duration and magnitude of seasonal-scale evaporative droughts. *Environ. Res. Lett.*, **11**, <https://doi.org/10.1088/1748-9326/11/10/104012>.
- Ukkola, A. M., A. J. Pitman, M. Decker, M. G. De Kauwe, G. Abramowitz, J. Kala, and Y. P. Wang, 2016b: Modelling evapotranspiration during precipitation deficits: Identifying critical processes in a land surface model. *Hydrol. Earth Syst. Sci.*, **20**, 2403–2419, <https://doi.org/10.5194/hess-20-2403-2016>.

- Wilhite, D. A., M. D. Svoboda, and M. J. Hayes, 2007: Understanding the Complex Impacts of Drought: A Key to Enhancing Drought Mitigation and Preparedness, <https://doi.org/10.1007/s11269-006-9076-5>.
- Xia, Y., and Coauthors, 2012: Continental-scale water and energy flux analysis and validation for the North American Land Data Assimilation System project phase 2 (NLDAS-2): 1. Intercomparison and application of model products. *J. Geophys. Res. Atmospheres*, **117**, n/a-n/a, <https://doi.org/10.1029/2011JD016048>.
- Yang, Z., 2013: Developing a flash drought indicator for the US Great Plains. University of Texas at Austin, 31pp., <http://hdl.handle.net/2152/21828>.
- Yang, Z.-L., and Coauthors, 2011: The community Noah land surface model with multiparameterization options (Noah-MP): 2. Evaluation over global river basins. *J. Geophys. Res.*, **116**, D12110, <https://doi.org/10.1029/2010JD015140>.
- Yuan, X., L. Wang, and E. F. Wood, 2018: Anthropogenic intensification of southern African flash droughts as exemplified by the 2015/16 season. *Bull. Am. Meteorol. Soc.*, **99**, S86–S90, <https://doi.org/10.1175/BAMS-D-17-0077.1>.
- Zaitchik, B. F., J. A. Santanello, S. V. Kumar, and C. D. Peters-Lidard, 2013: Representation of soil moisture feedbacks during drought in NASA unified WRF (NU-WRF). *J. Hydrometeorol.*, **14**, 360–367, <https://doi.org/10.1175/JHM-D-12-069.1>.
- Zhang, Y., Q. You, C. Chen, and X. Li, 2017: Flash droughts in a typical humid and subtropical basin: A case study in the Gan River Basin, China. *J. Hydrol.*, **551**, <https://doi.org/10.1016/j.jhydrol.2017.05.044>.
- Zhang, Y., T. F. Keenan, and S. Zhou, 2021: Exacerbated drought impacts on global ecosystems due to structural overshoot. *Nat. Ecol. Evol.* **2021 511**, **5**, 1490–1498, <https://doi.org/10.1038/s41559-021-01551-8>.